This is the final draft of the contribution published as:

Dávila-Jiménez, M.M., Elizalde-González, M.P., **Guerrero-Morales, M.A.**, **Mattusch, J.** (2018):
Preparation, characterization, and application of TiO_2/Carbon composite: Adsorption, desorption and photocatalysis of Gd-DOTA
Process Saf. Environ. Protect. **120** , 195 - 205

The publisher's version is available at:

http://dx.doi.org/10.1016/j.psep.2018.09.012

Preparation, characterization, and application of TiO_2/Carbon composite: Adsorption, desorption and photocatalysis of Gd-DOTA

Martín M. Dávila-Jiménez[a]

María P. Elizalde-González[b, *]

maria.elizalde.uap.mx@gmail.com

Mario A. Guerrero-Morales[b, c]

Jürgen Mattusch[c]

[a]Facultad de Ciencias Químicas, Benemérita Universidad Autónoma de Puebla, Av. San Claudio y 18 Sur, Ciudad Universitaria, Puebla, Pue, 72570, Mexico

[b]Centro de Química, Instituto de Ciencias, Benemérita Universidad Autónoma de Puebla, Ciudad Universitaria, Edif. IC7, Puebla, Pue, 72570, Mexico

[c]Department Analytical Chemistry, Helmholtz Centre for Environmental Research – UFZ, Permoserstrasse 15, Leipzig, 04318, Germany

*Corresponding author.

Abstract

The preparation methodology of a photocatalytic acting composite consisting of TiO_2/Carbon carrying 24.5% of TiO_2 is described. The environmental friendly TiO_2/Carbon bifunctional material combining immobilized photocatalytic properties with a macroparticular carbonaceous ad-/desorbent was prepared in one-step procedure at low temperature from guava seeds and Ti(IV) oxysulfate as carbon and photocatalyst precursors, respectively. With artificial solar radiation, the composite can act as a photocatalyst for the degradation of the emerging pollutant, gadolinium-based contrast agent Gd-DOTA in aqueous solution with a degradation yield of 95%. For its reuse, the composite can be separated from the solution without centrifugation. The TiO_2/Carbon composite is also able to adsorb and desorb the non-complexed gadolinium (Gd^{3+}) ion once the cyclic Gd-DOTA is destroyed. The resulting photodegradation /-transformation as well adsorption and desorption phenomena were studied by analyzing the occurring Gd-species using ion exchange chromatography coupled to element and molecule selective mass spectrometers on-line (IEC-ICP-MS/ESI-QToF-MS).

Keywords: Photocatalyst; TiO_2; Adsorbent; Carbon; Gadolinium complex; Transformation (Eliminate "Transformation" and write instead: "Photoproducts of DOTAREM"); IC-ICP-MS/ESI-QToF-MS

1 Introduction

The aquatic environment is the priority destination of contaminants produced by hospitals, and the level of growth is revealed by sensitive analytical methods developed in recent years (Aga, 2008; Birka et al., 2016a). Anthropogenic gadolinium is an emerging pollutant in the waters around the world (Zhu et al., 2004; Bau et al., 2006; Lawrence et al., 2009; Rabiet et al., 2009), and its concentration increased in the tap water of the western districts of Berlin and along the Rhine River between 2009 and 2012 as a result of the use of gadolinium-based contrast agents (GBCAs) required in magnetic resonance imaging (MRI) (Tepe et al., 2014). In Switzerland alone, the extrapolated consumption of GBCA was 157 kg of gadolinium per year (6728 MRI treatments in one hospital) (Kuroda et al., 2016). Correspondingly, the number of expositions to Gd-DOTA was 5400 in a Mexican hospital in 2017 (personal communication). Additionally, the gadolinium concentration coming from GBCAs in the wastewater of a cantonal hospital in Switzerland was 13.4 µg L^{-1} before treatment in a membrane bioreactor and 12.9 µg L^{-1} after handling in the bioreactor, indicating the inefficiency of the treatment (Kovalova et al., 2013).

The contrast agent gadoterate meglumine or gadoteric acid (Gd-DOTA (Please eliminate completely the minus sign.)$^-$) is a macrocyclic and ionic gadolinium-based ~~molecule~~complex (M = 753.86 g ~~mol~~ mol^{-1}). This GBCA has a predominant renal elimination and a mean plasma elimination half-life of 91 ± 14 min (Soyer et al., 2017), an osmolality of 1.35 mol~~L~~ kg^{-1}, a predicted log P of -7.6, a pK_a (strongest acidic) of 0.47, a pK_a (strongest basic) of 10.08 and a physiological charge of -2 (Drugbank, 2017). Gd-DOTA is characterized by excellent chelate stability and low risk for nephrogenic systemic fibrosis (NSF) (Wagner et al., 2016). Since free gadolinium is released from GBCAs via transmetallation, it is believed that in the bodies of patients with renal dysfunction, this process is the most important cause of NSF. Recently, the European Medicines Agency (EMA) restricted the use of linear Gd-contrast agents and has only been approved for selected treatments, which will hopefully reduce the incidence of systemic fibrosis and other potentially risks associated with gadolinium depositions in brain (EMA, 2017). In this manner, some efforts have

focused on the removal of free gadolinium and GBCAs from dialysate and blood with nanostructured silica materials, for example (Yantasee et al., 2010). However, with or without transmetallation, gadolinium and gadolinium-containing compounds get into the water via hospital wastewater.

Until now, insufficient research has been devoted to the removal of GBCAs by adsorption (Kovalova et al., 2013; Cyris, 2013; Elizalde-González et al., 2017). Cyris (2013) reported 41% removal efficiency of the GBCA called Gd-DTPA-BMA for a dosage of 10 mg L^{-1} on the commercial carbon Norit SA UF (1200 $m^2 g^{-1}$), and Kovalova et al. (2013) could not adsorb GBCAs on powdered activated carbon using the same dose. By controlling mesoporosity and surface charge of the carbon samples, we were able to adsorb 70–90% of three GBCAs in the concentration range of 0.5–6 mM in aqueous solution and less in model urine (Elizalde-González et al., 2017).

Studies on sewage treatment of GBCAs are scarce and have yielded low removal of gadolinium (Telgman et al., 2012). Among the oxidative treatments, photolysis failed (Kovalova et al., 2013), ozonation was either not successful (Kovalova et al., 2013) or was very slow and ineffective (Cyris, 2013), whereas H_2O_2 was fast (Cyris, 2013), and UV irradiation degraded only Gd-BOPTA (gadobenate dimeglumine, MultiHance™) (Birka et al., 2016b). Since the last two procedures released toxic free gadolinium, removal of free gadolinium must also be considered to improve the safety of the treatments. Other researchers have tested the removal of Gd^{3+} by activated charcoal (Qadeer et al., 1992), graphene (Chen et al., 2014), chitosan/carbon nanotubes (Li et al., 2015), silica (Gao et al., 2017) and titanium dioxide (Liang et al., 2001; Khalid et al., 2017; Khaki et al., 2017). The photocatalyst TiO_2 has not been considered yet in handling GBCAs probably due to the difficulties associated with their handling both in reactors and tanks.

Combination of the photocatalyst TiO_2 immobilized on activated carbon improved the adsorption efficiency and therefore the photocatalytic activity too (Alipour et al., 2018). The first attempt to synthesize a carbon-titanium dioxide composite used wood carbon and $TiCl_4$ (Ermolenko and Yatsevskaya, 1970). Later, Uchida et al. (1993) prepared TiO_2 supported on activated carbon by the sol-gel method and Ding et al. (2001) by chemical vapor deposition. The joint use of TiO_2 and activated carbon was firstly reported by Matos et al. (1998) for the photodegradation of phenol. Stirring suspended particles of TiO_2 together with porous carbons in the reaction setup was performed in numerous research works of this group transiting through experiments with bicomponent powders (Matos et al., 2010) until the preparation of a carbon-doped TiO_2 material (Matos et al., 2017) yielding always microparticles requiring filtration and/or centrifugation.

Therefore, the present work focused on the development of a process for the effective photodegradation of Gd-DOTA combined with the removal of gadolinium species formed from treated aqueous solutions and synthetic urine using photocatalysis by a TiO_2-carbon granular composite with the aim of analyzing under which circumstances toxic Gd species can be eliminated from the solution.

2 Material and methods

2.1 Chemicals

Titanium (IV) oxysulfate (Sigma-Aldrich, Darmstadt, Germany) and glycerol GR (87%, Merck, Darmstadt, Germany) were used as reagents. Ammonium hydroxide (28%, Aldrich, St. Louis, MO, USA) was used to form the titanium gel. Guava seeds of natural sizes were used as a carbon source. The chemical composition of guava seeds was reported previously (Elizalde-González and Hernández-Montoya, 2009). Titanium (IV) oxide anatase phase (99.7%, Sigma-Aldrich, Darmstadt, Germany) and rutile phase (99.99% ABCR GmbH, Karlsruhe, Germany) were used. Ammonium acetate for analysis was obtained from Merck Millipore (Darmstadt, Germany), and de-ionized water (18.2 MΩ cm, DirectQTM 5 system) was obtained from Millipore. The Gd-DOTA (gadoteric acid) contrast agent DOTAREM® was provided by Guerbet (Roissy, France). All results are referred to the gadoteric acid ($C_{16}H_{28}GdN_4O_8$, M 561.668 g mol^{-1}) concentration certified in the 10 mL flask corresponding to 279.32 $mg_{Gd\text{-}DOTA}$ mL^{-1} (0.5 $mmol_{Gd\text{-}DOTA}$ mL^{-1}). The ethylenediaminetetraacetic acid disodium salt dihydrate (EDTA) ligand was purchased from Mallinckrodt (St. Louis, MO, USA). The graphitic material Carbopack C™ (Sigma Aldrich, Darmstadt, Germany) was used for comparison.

2.2 Preparation of the TiO_2/Carbon composite

Whole guava seeds used in this work were discarded by a juice and jelly factory. Raw seeds (500 g) of natural sizes (average length 2 mm and width 1.5 mm) were added to a 20% solution of titanium (IV) oxysulfate in a 5% glycerol aqueous solution and stirred for 12 hours. Then, 100 mL of NH_4OH (25%, Suprapure, Merck) was added dropwise. The gel was transferred immediately to a rotary tubular furnace Model OTF-1200X from MTI Corporation (Richmond, CA, USA) with a quartz reactor. Carbonization was performed under an air flow of 1.25 L min^{-1}. The heating gradient started from 25 to 250 °C at 4 °C min^{-1} for 60 minutes and continued from 250 to 500 °C at 2 °C min^{-1} for 3 hours. The carbonaceous constituent of the TiO_2/Carbon composite prepared in this way occurs as thermally “activated carbon” and for simplicity is called “Carbon”. Guava carbon was prepared under the same conditions for comparison with the composite performance. The granules of the carbon and the composite were stirred (200 rpm) in water for 2 hours for microscopic examination.

2.3 Characterization of the composite

2.3.1 Scanning electron microscopy and elemental composition

The composition of the sample on the surface was determined using an EDS spectrometer (Oxford Instruments INCAX-act Energy 350) coupled to a scanning electron microscope (SEM) (JEOL JSM 6610 LV). The elemental composition was

estimated by mapping clockwise on 10 sites of the granules. The bulk titanium content was determined in triplicate using wavelength dispersive X-ray fluorescence using a Bruker S8 TIGER (Billerica, MA, USA) spectrometer. The particles were ground and mixed with 20% Hoechst wax C micro-powder to form tablets.

2.3.2 Vibrational and electronic spectroscopic methods

The Raman spectra were measured with a Renishaw inVia Raman microscope at 633 nm (Gloucestershire, England). The spectra were recorded with a power of 0.8 mW for 10 and 20 ~~second~~s. Functional groups were titrated with the help of Metrohm Titrando 809 equipment (Herisau, Switzerland). A Nicolet 6700 IR spectrophotometer was used to record in triplicate FTIR transmission spectra in KBr pellets with the same sample concentration in all cases. Attenuated total reflection (ATR) spectrum was also recorded with the same instrument. UV-~~VIS~~vis diffuse reflectance spectra (DRS) of three ground composite samples were recorded at room temperature using an AvaSpec 2048 L spectrometer from Avantes Inc. (Louisville, CO). A Kratos AXIS Nova X-ray photoelectron spectrometer was used for the XPS analysis of the ground sample. XPS survey spectra were obtained from an area of approximately 300 x 700 µm using a pass energy of 160 eV. XPS high resolution (HR-XPS) spectra were obtained from an area of approximately 300 x 700 µm using a pass energy of 20 eV.

2.3.3 Determination of surface area and functional groups of the composite

The BET surface area was measured by nitrogen adsorption at 77 K using a texture analyzer instrument (Autosorb-1 from Quantachrome, Florida, USA) after out-gassing at 573 K for 24 h~~ours~~. The specific surface was calculated using non-local density functional theory, and the pore size distribution was estimated by the Barrett–Joyner–Halenda method (BJH). Functional groups and point of zero charge were determined by potentiometric mass titration (Fiol and Villaescusa, 2009) using a 809 Titrando from Metrohm (Herisau, Switzerland).

2.4 Photocatalytic experiments under artificial solar irradiation

A Q-SUN Xe-1B (Q-Lab GmbH, Saarbrücken, Germany) equipment with a sun light simulating xenon lamp and daylight-Q filter using a continuous spectrum of 280-800 nm was used as radiation source. The irradiance intensity was calibrated to 0.68 W m^{-2} at 340 nm for constant radiation. The total UV~~-vis irradiance in the range of 280 to 800 nm was 768 W m-~~-vis-irradiance in the range of 280–800 nm was 768 W m^{-2}. The radiation chamber was thermostated at 32 °C. The reactor was equipped with a quartz cell (10 mL) and tubing to allow for the bubbling of air into the solution. Most of the experiments reported here were performed without the input of air, whereas in selected trials, air was bubbled into the cell to stir the composite particles and to stabilize the oxygen content. The entire assembly was enclosed in the chamber with several doses of the TiO_2/Carbon photocatalyst and a constant initial concentration of Gd-DOTA (1 mg L^{-1}) and the normal set-up of the Q-Sun was used. In photocatalysis with TiO_2 nanoparticles three doses of the solid photocatalyst were used: 1 g L^{-1} with rutile, 0.1 g L^{-1} with anatase and 0.01 g L^{-1} with anatase and stirring. In the experiments with the TiO_2/Carbon composite the following doses were used: 8, 17 and 34 g L^{-1}. The irradiation was started by switching on the extended UV-quartz mode. Depending on the degree of photodegradation, variable radiation duration was chosen for the experiments. Aliquots of 100 µL were collected at regular time intervals during the irradiation and were subsequently analyzed using ion exchange chromatography with an inductively coupled plasma mass spectrometric detector (IEC-ICP-MS).

2.5 Liquid chromatography for analysis of photocatalytic products

IEC-ICP-MS was conducted to separate those photolysis products containing gadolinium, using optional a Dionex IonPac AS9HC column (250 × 4 mm) (Dionex, Sunnyvale, USA) and Dionex IonPac AS23~~--~~-4 µm (250 x 2 mm) (Thermo Scientific). Bi-distilled water (Eluent A) and a 0.5 M ammonium acetate solution (Eluent B) were used as mobile phase at a flow rate of 1 mL min~~-1 (AS9HC) and 0.25 ml min-~~$^{-1}$ (AS9HC) and 0.25 mL min^{-1} (AS23). Gradient elution was performed from 1~~-~~ to 10% B in 15 min for AS9HC and in 45 min for AS23. The injection volume was 20 µL in both cases.

The photocatalytic process was monitored sequentially with an HPLC-ICP-MS instrument consisting of a µ–LC series 1200 chromatograph (degasser, binary pump, thermostated autosampler) coupled with an ICP-MS series 7500ce detector from Agilent Technologies, Santa Clara, CA, USA). The detection mass was *m/z* 157 (Gd^+). To identify the transformation products of Gd-DOTA and the gadolinium species after desorption, a dual detection coupled to HPLC (HPLC-ICP-MS/ESI-QToF-MS) was used. The instrument configuration consisted of an UPLC Series Infinity 1290 (Degasser, binary pump, thermostated autosampler) coupled with an ICP-MS 7500ce and Accurate QToF LC/MS 6530 in parallel (all from Agilent Technologies, Santa Clara, USA) by splitting the mobile phase (1:4=ICP-MS:ESI-MS) with an adjustable flow splitter from Analytical Scientific Instruments (CA, USA). To quantify Gd ions in solution, an external calibration curve using the peak areas of the ICP-MS detection in the concentration range 0.5~~– 2.0 mg L-1 of Gd-DOTA (0.14 – 0.56 mg L-~~-2.0 mg L^{-1} of Gd-DOTA (0.14–0.56 mg L^{-1}) was constructed: Area = 14140C (R^2 = 0.9991). IEC-ESI/QToF-MS measurements were used to identify the transformation products by their (I) accurate masses-to-charge ratios (*m/z*) (R = 10~~000–15~~,000-15,000) with an error < 5 ppm, (II) isotopic pattern of Gd and (III) comparison with the retention times of the parallel monitored ICP-MS signals. The ICP-MS detection can be interfered by TiO_2 nanoparticles present in the analyte solutions. Therefore, suspended anatase nanopowder with particle size <25 nm has to be removed carefully from solutions by ultrafiltration or centrifugation.

2.6 Adsorption-desorption experiments

Adsorption tests were performed at room temperature in the concentration range of 300 ~~to 1900 mg L-~~ -1900 mg L^{-1} in batch experiments in darkness. The graphite and the composite were dried for 24 h ~~ours~~ at 50 °C. Then, each material was weighed into polycarbonate cylindrical cells with lids, and Gd-DOTA solutions were placed in contact with the materials in absence of light. The following m/V ratio was probed: 34 g L^{-1}. In order not to affect the adsorption by higher concentrated buffer components the pH was not adjusted. After 12 h ~~ours~~, the adsorption reached equilibrium, and then the solution was separated and analyzed using the IEC-ICP-MS technique as described above. For desorption after photodegradation, the exhausted composite was shaken for 1 h ~~our~~ in an ethanol-water (1:1) solution. An aliquot of 500 µL was taken, and after adding 5 µL of a 3 mM EDTA, the solution was analyzed by IEC-ICP-MS / -ESI-QToFMS.

3 Results and discussion

3.1 Characterization of the TiO_2/Carbon composite

Combining photocatalysis and adsorption in a composite material plays an important role for effective degradation and removal of pollutants (Khaki et al., 2017; Alipour et al., 2018). In this work the carbon–based bifunctional composite was created to interlock the ad- /desorption properties of activated carbon with the photodegradation ability of TiO_2 immobilized and finely dispersed on the irregular carbon surface. As an additional technical aspect is to mention the ease of recovery, because the composite with particle sizes of 1 to 3 mm in diameter can be separated by paper filtration or sedimentation effortlessly from the reaction solution than if colloidal TiO_2 nanoparticles (size range: 20-50 nm) would be deployed. From ecological point of view unused waste products of sustainable vegetable materials as starting material were modified to obtain the appropriate material properties.

The TiO_2/C-composite was characterized by SEM-EDX, Raman, FTIR, DR-~~UV-Vis~~ UV-vis- spectroscopy and texture analysis. In parallel and for comparison, some studies were conducted with the carbonized seeds without TiO_2 adhered to the surface. Both the composite and the blank carbon were dark gray glossy granules. Optical microscopy confirmed white layers on the granules depicted in Fig. 1A with average weight 5.2 ± 0.4 mg (N = 10).

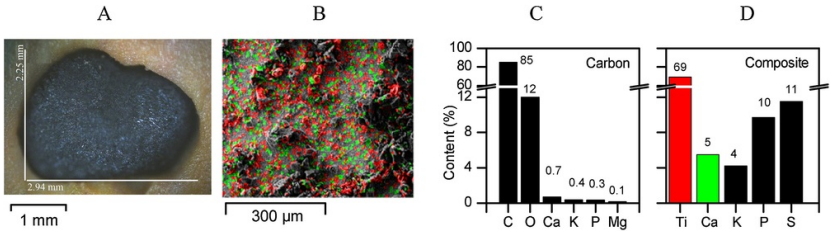

Fig. 1 Micrograph of a composite´s (must read "composites grain") grain (A) and SEM image (B) of its surface: Red dots represent Ti, green dots indicate Ca. SEM-EDX results of the carbon (C) and TiO_2/Carbon composite (D) prepared from guava seeds (For interpretation of the references to colour in this figure legend, the reader is referred to the web version of this article.).

alt-text: Fig. 1

Fig. 1B shows the scanning electron microscopic image (SEM) of the composite´s surface over an area of ca. 500 x 500 µm. Fig. 1C contains the composition results obtained from the energy-dispersive X-ray (EDX) spectra of the guava carbon surface with traces of the endogenous elements Ca, Mg, K, and P in concentrations similar to those published by Uchôa-thomaz et al. (2014) except that of Ca. In addition to carbon, the presence of oxygen (12%) indicates the occurrence of oxygen-containing functional groups generated presumably by thermal processes during thermal treatment of the guava seeds. In the semi-quantitative analysis of the composite´s surface, when the main elements, carbon and titanium are not considered, the oxygen content rises to 98% and is distributed both in the surface groups of the carbon and in the titanium dioxide. Fig. 1D shows that among the elements quantified on this composite ´s (This genitive form is correct. It must read "composite´s" In the proof as pdf file it appears different (accented consonant s). Please check.) (This genitive form is correct. In the proof as pdf file it appears different (accented consonant s). Please check.)surface (excluding carbon and oxygen), titanium (red dots in Fig. 1B) exhibits 69% and calcium (green dots in Fig. 1B) 5%.

The quantity of sulfur in the composite arises from the titanium (IV) oxysulfate reagent used in the preparation of the composite. Besides surface analysis, bulk determination of the TiO_2 load in the composite´s (This genitive form is correct. In the proof as pdf file it appears different (accented consonant s). Please check.)granules was performed by XRF analysis. It revealed that the titanium content on the composite was 14.7 ± 0.6% on average (see Table 1), which corresponds to 24.5% TiO_2. Our SEM images suggest that photocatalysis and adsorption-desorption phenomena should take place on this composite due to the coexistence of TiO_2 and carbon zones on the surface.

Table 1 (The lines below the first-line headings are not grouping correctly the parameters. I attach the Table.)Structural and textural characteristics of the guava carbon and the TiO_2/carbon composite prepared from guava seeds.

alt-text: Table 1

Sample	Ti (%)	Raman phonons Δω (cm⁻¹)						Textural parameters		pH_{pzc}
		G	D	E_g	A_{1g}	B_{1g}	E_g	S_{NLDFT} ($m^2\ g^{-1}$)	$V_{<1\ nm}$ ($cm^3\ g^{-1}$)	
Carbon	—	1586	1359	—	—	—	—	640	0.186	6.7
Composite	14.7 ± 0.6	1587	1363	639	517	397	146	97	0.020	6.6

After one-step carbonization-calcination at 500 °C, the composite prepared via titanium (IV) oxysulfate was analyzed by X-ray diffraction and Raman spectroscopy to identify the anatase phase of the immobilized TiO_2. Spectrum of the composite in Fig. 2A shows the main active modes of the anatase structure with the characteristic Raman shift (Sekiya et al., 2001) at 639, 517, 397 and 146 cm^{-1} that has the highest photocatalytic activity (Luttrell et al., 2014). The corresponding symmetry modes are given in Table 1. The positions of the bands shifted slightly from the positions of an anatase monocrystal. However, no bands corresponding to the rutile phase (Frank et al., 2012) were present in the composite prepared using titanium (IV) oxysulfate. The G and B bands of the carbon in both the guava carbon (spectrum in dotted line) and the composite (spectrum in continuous line) can also be observed. The parameters expressing the structural order degree in the carbonaceous matrix of the composite were: $I_D/I_G = 3.1$ and $I_D/(I_D+I_G)x100 = 75\%$. The peak shown in the inset in Fig. 2 (must read "Fig. 2A")is broad and is similar to that observed in diffractograms of a sample of activated carbon obtained from orange peel (Xie et al., 2014). Nevertheless, it may overlap the anatase reflection at 2θ of 25.28 degrees in the X-ray diffractogram of the composite (Zeng et al., 2010).

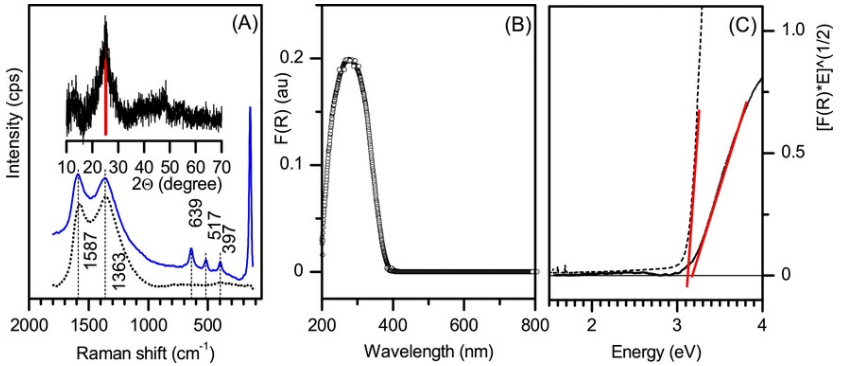

Fig. 2 Raman spectrum of the composite (continuous line) and the carbon (dotted line) (A). Insert in (A): X-ray diffractogram. DRS spectrum (B) of the composite and Tauc plot (C) of TiO_2 (dotted line) and the TiO_2/Carbon composite.

alt-text: Fig. 2

Fig. 2B shows the DRS spectrum of the composite which served to investigate the change in the band gap of anatase when loaded on guava carbon. The phonon energy obtained by means of extrapolation of the Kubelka-Munk function showed no quantitative change in Fig. 2C since the band gap was 3.10 eV for TiO_2 and 3.15 eV for the composite.

Fig. 3A shows Fourier transform infrared spectroscopy (FTIR) spectra of the composite. The broad band appearing at 3407 cm^{-1} ~~1 is ascribed to O–H or N–~~ $^{-1}$ is ascribed to O–H or N–H stretching vibrations of secondary amines. The group of three small bands in the 2923 cm^{-1} ~~1 region corresponds to C–~~ $^{-1}$ region corresponds to C–H stretching vibrations of alkanes and alkenes. The sample also exhibits a N–H bending vibrations at 1597 cm^{-1}. This last band might overlap the Ti–O–H characteristic band at 1639 cm^{-1} and the lattice vibration of TiO_2 is present at 1434 cm^{-1} (Foratirad et al., 2017) involved in a broad band of the guava carbon (Elizalde-González and Hernández-Montoya, 2009). The band in the range 925–400 cm^{-1} involves the Ti–O vibrations centered at 600 cm^{-1} (Vijayalakshmi and Sivaraj, 2016). The C 1 s XPS spectrum of the composite (Fig. 3B) indicates the presence of five types of carbon bonds: aromatic C–C, C–H (285.00 eV), ~~C = C (284.50 eV), C–OH, C–O–C (286.50 eV), C = O (287.90 eV), and O~~ C, C–H (285.00 eV), C = C (284.50 eV), C–OH, C

O

C (286.50 eV), C

O (287.90 eV), and O

C = O (289.00 eV). The high resolution XPS spectrum shown in Fig. 3C demonstrates the presence of two N 1 s nitrogen species in similar amounts: 54.4% at 400.59 eV and 45.6% at 398.78 eV. This result, together with the FTIR spectrum evidenced the presence of nitrogen, probably associated with carbon and/or oxygen. The formed nitrogen species can come both from the NH_4OH used in the preparation of the composite and from the raw guava seeds (1.5%) (Elizalde-González and Hernández-Montoya, 2009). Besides, the two peaks, Ti (2p1/2) and Ti (2p3/2), at 465.1 (36%) and 459.4 eV (64%) indicate that the titanium cation is in Ti^{4+} covalent state (Fig. 3D). The splitting between these two bands is 5.69 eV. Since the Ti core-level XPS spectrum of TiO_2 exhibits peaks at 464.0 and 458.3 eV with the same splitting of 5.7 eV, this implies that the shift of the peak positions in our sample (1.1 eV) to higher energy values may be attributed to the interaction of Ti(IV) with groups of the guava carbon, i.e. electronegative oxygen and nitrogen atoms. This effect has been observed in TiO_2-reduced graphene oxide nanocomposites (Shah et al., 2012). Further, we compared the 398.78 eV peak in Fig. 3C with the N 1 s (N–Ti) peak in titanium nitride. The value of 398.78 eV observed in our sample is higher than that reported by Asahi et al. (2001) for films and powder of nitrogen-doped titanium dioxide (396 eV) and by Jaeger and Patscheider (2012) for crystalline TiN epitaxially grown (397.11 eV). As in the case of the binary composite TiO_2-activated carbon prepared by Matos et al. (2017), we did not observe a peak corresponding to the chemical bond Ti–C by considering that XPS has detection limits ranging from 0.1 to 0.5 atomic percent depending on the element. Quantification of the composite groups and elements is not reported here since XPS analyses the probe to a depth of 7–10 nm and we performed a bulk analysis by XRF to determine the titanium content (14.7%) as discussed in section 3.1.

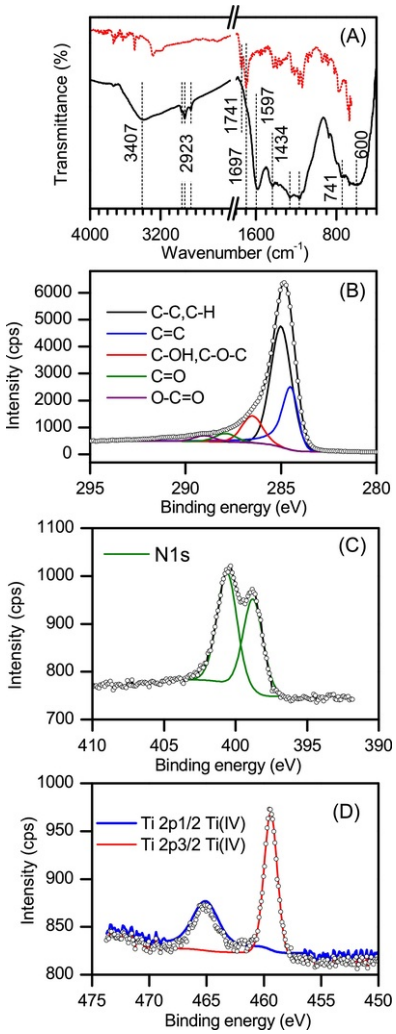

Fig. 3 Transmission (continuous line) and total attenuated reflection (dashed line) FTIR spectra (A) and high resolution XPS (B–D) spectra of the prepared TiO_2/Carbon composite.

alt-text: Fig. 3

The carbon and its composite showed type Ia nitrogen adsorption isotherms according to the refined IUPAC classification (Thommes et al., 2015). This indicates the presence of narrow micropores, and despite microporosity, the specific surface magnitudes were less than 650 $m^2 g^{-1}$ due to the large granule size (1.5 mm). The nitrogen adsorption isotherms are shown in Fig. 4A. The values of the specific surface areas are listed in Table 1. The presence of crystalline TiO_2 affected the specific surface area with respect to the nude carbon obtained from the guava seeds (Table 1). This indicates that the titanium (IV) oxide nanoparticles block the narrow micropores in some parts of the surface as $V_{\mu<1nm}$ decreased from 0.186 in the carbon to 0.082 $cm^3 g^{-1}$ in the composite. The micropore distribution curves in Fig. 4B show the fraction of narrow micropores remaining in the composite.

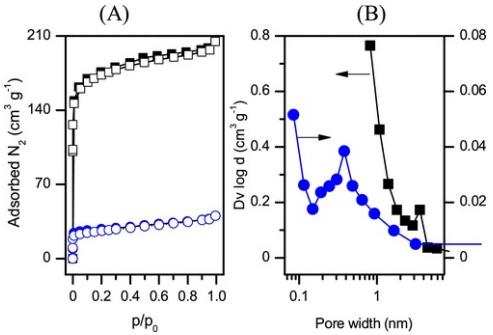

Fig. 4 Nitrogen adsorption (empty symbols) and desorption (full symbols) isotherms (A) of the guava carbon (squares) and the TiO_2/Carbon composite (circles) and micropore distribution (B).

alt-text: Fig. 4

Fig. 5 presents the distribution of acidic and basic groups in the carbon and the composite, which are both lightly acidic judging from the pH_{pzc} values (Table 1). The potentiometric titration (González-Guerrero et al., 2008; Boehm, 2002) reveals that the functional groups of the guava seed carbon are mostly acidic (44%) and predominantly of a carboxylic acid type, whereas in the composite, they amount to 59%. The neutral lactonic and phenolic groups in the pH range 6–8 almost disappear in the composite (9%) compared to the guava carbon (40%).

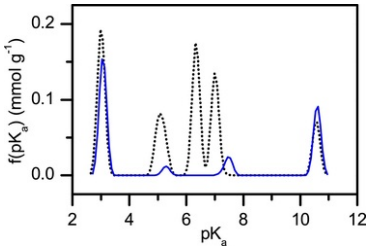

Fig. 5 pK_a distribution for the surface groups of the guava carbon (dotted lines) and the TiO_2/carbon composite (continuous lines) prepared from guava seeds.

alt-text: Fig. 5

XPS revealed the following relative abundance of C 1 s groups in the composite: C

—

~~C, C–H > C=C > C–OH, C–O–C > C=O > O–C=~~C, C

—

H > C

=

C > C

—

OH, C

—

O

—

C > C

=

O > O

—

C

=

O. Here, the lower amount of carbonyl groups accounts for the basic properties and the hydroxyl moiety for the acidic properties of the composite. Interestingly, no clear carbonyl group was observed in the FTIR transmission spectrum of the composite because depending on the type of compound, the stretching vibration of C

=

~~=~~O can appear within 1780 and 1550 cm^{-1} and could be masked in Fig. 3A (continuous line). The ester and ketone (or amide) carbonyl bands were detected by ATR (Fig. 3A, dashed line) at 1741 and 1697 cm^{-1}, respectively.

The finding of the C
=
-C, C-H and C=C, C-H and C
=
C groups by XPS analysis agrees with the alkanes and alkenes bands observed by FTIR spectroscopy and correspond to the composites skeletal carbon not contributing to the acidic-basic properties.

3.2 Comparison between photolysis and heterogeneous photocatalysis of Gd-DOTA

The photocatalytic activity of the here presented TiO_2/Carbon composite was tested on the transformation of Gd-DOTA and compared with photocatalysis experiments carried out with TiO_2 (both rutile and anatase phase). In both cases a heterogeneous photocatalysis takes place whether as dispersed semiconductor nanoparticles of TiO_2 in fine dispersed slurry or on TiO_2/Carbon composite. For comparison, the direct photolysis of Gd-DOTA was performed under the same irradiation conditions. Fig. 6A illustrates the kinetic curves describing the rate of photolysis and photocatalysis of Gd-DOTA (1 mg L^{-1}) using two commercially available TiO_2 photocatalysts. The diminution of the Gd-DOTA peak area with time was measured by IEC-ICP-MS on *m/z* 157 (Gd^+). For other substrates, it has been demonstrated that the photocatalytic activity of anatase is higher than that of rutile (Zhang et al., 2014). Also in the present case, photocatalysis of Gd-DOTA by anatase was much more efficient than by rutile even if a 100-fold dose of the photocatalyst was used (Fig. 6A). Photolysis also decomposed Gd-DOTA to 96% within 20 hours, and photocatalysis with suspended rutile decomposed Gd-DOTA to a steady state of 81% after 24 hours. To observe the influence of stable oxygen content, air was bubbled into the cell. With air bubbles a tenth of the anatase mass exhibited the same performance as without air: Gd-DOTA was completely removed within 3 hours (Fig. 6A). With the TiO_2/Carbon composite prepared in this work, photocatalysis with different doses (8, 17, 34 g L^{-1}) led to a decrease of Gd-DOTA concentration and a calculated photodegradation yield of 73–95%, respectively, after 9 hours of exposure (Fig. 6B). After the experiment, the composite granules could be easily separated from the solution by a simple decantation step. Kinetic parameters were calculated from the exponential expression resulting after integration of the *pseudo*-first order kinetic model with boundary conditions and not by the conventional linear regression of the equation [$ln(C_{equil} - C_t) = lnC_{equil} - k_1 t$], yielding the rate constants gathered in Table 2 ($R^2 = 0.99$ and $\chi^2 = 5\ 10^{-4}$). Despite the high photodegradation rate of Gd-DOTA observed by using the composite, the rate constant k_1 could be increased further, and the $t_{1/2}$ values could be decreased by a factor of 2 when air was bubbled through the photoreactor to improve the mass transfer to the composite particles and possibly to adjust the oxygen content (see Table 2). Under artificial solar irradiation, the highest efficiency obtained by suspended anatase and its high photodegradation rate could nearly be achieved by the proposed composite material.

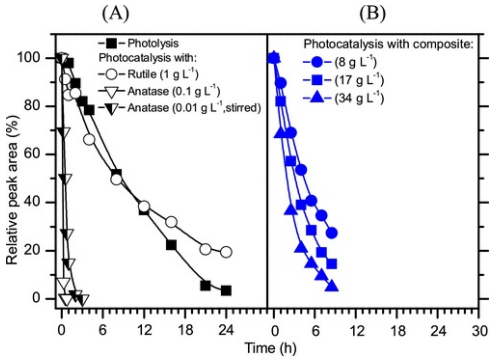

Fig. 6 Concentration decay of an aqueous solution of Gd-DOTA (1 mg L^{-1}) subjected to artificial solar light radiation in presence of different photocatalysts (A) and the composite (B) in different doses.

alt-text: Fig. 6

Table 2 Kinetic parameters of the photodegradation of Gd-DOTA (1 mg L^{-1}) aqueous solution on the prepared TiO_2/Carbon composite exposed to artificial solar radiation under static and dynamic conditions induced by stirring with air bubbles.

alt-text: Table 2

Photocatalyst dose (mg mL^{-1})	Static system			Dynamic system		
	k_1 (min^{-1})	$t_{1/2}$ (min)	Removal (%)	k_1 (min^{-1})	$t_{1/2}$ (min)	Removal (%)
34	0.006	117	95	0.015	46	97
17	0.004	180	86	0.008	86	85

8	0.003	270	73	0.004	157	74

3.3 Adsorption experiments with Gd-DOTA and its phototransformation products

The adsorption of Gd-DOTA on activated carbon was investigated recently by Elizalde-González et al. (2017). The surface of the TiO_2/Carbon composite used in this work exposes considerable carbonaceous zones. To determine if the decrease in the Gd-DOTA concentration occurred due to photocatalysis (adsorption, photocatalytic degradation, desorption) on immobilized TiO_2 nanoparticles or mainly by adsorption on the uncovered porous carbon, the composite's capacity to adsorb Gd-DOTA was studied in the dark. The concentration range used for the measurement of the adsorption isotherm was selected according to the probable concentration in 2 L excreted urine after an application of 1.2 to 3.6 g/patient. A complete adsorption isotherm of Gd-DOTA on the prepared composite in the concentration range of 300~~-1900 mg L-~~-1900 mg L^{-1} at 298 K is presented in Fig. 7A. Adsorption of this GBCA does not occur in the low concentration range, and only begins at 1000 mg L^{-1} equilibrium concentration C_{equil} (use italics in the whole word "equil". It seems that the last "l" is not italic font.) of Gd-DOTA. In terms of surface charges, the composite (pH_{pzc} 6.6) carries a slight positive charge at the pH of Gd-DOTA in water (pH 6.4), since $pH_{pzc} \geq$ pH (Parfitt and Rochester, 1983). Then, $GdH_2(DOTA)^+$, the prevailing species of Gd-DOTA at pH 6.4 (Elizalde-González et al., 2017), experimentally undergoes electrostatic repulsion against the surface and interacts only by dispersive forces. This isotherm can be categorized as an S-type isotherm according to Giles isotherm classification. When adsorption on carbon occurs in water, this behavior is in line with bifunctional adsorbates carrying both a non-polar and polar moiety (Giles et al., 1960). For comparison, the adsorption isotherm of Gd-DOTA on graphite (Fig. 7A) exhibits a weak adsorption in the low concentration range and saturation (Type L form), which is characteristic of adsorbates that are most likely adsorbed flat. This significant difference in the forms of the adsorption isotherms is due to the characteristic absence of functional groups on some commercial graphite surfaces not subjected to any kind of treatment.

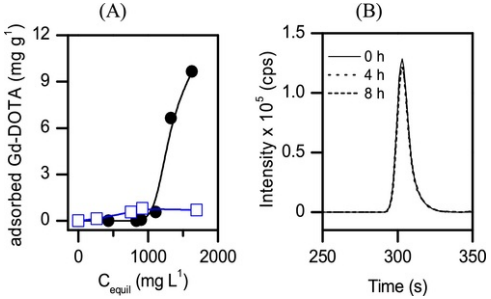

Fig. 7 Adsorption isotherms (A) of an aqueous solution of Gd-DOTA on the TiO_2/Carbon composite and on graphite. HPLC-ICP-MS chromatograms (B) of Gd-DOTA (1 mg L^{-1}) in water after 8 h~~ours~~ exposure to artificial solar light in presence of guava carbon. Solid dose: 34 g L^{-1} (A and B). Empty squares – graphite, full circles – composite.

alt-text: Fig. 7

As mentioned in the previous section, the adsorption of Gd-DOTA was evaluated using IEC-ICP-MS analysis. As seen in Fig. 7B, the peak of Gd ($m/z = 157$) (as Gd-DOTA, 1 mg L^{-1}) remained unchanged after contact of Gd-DOTA with the pure guava carbon (34 g L^{-1}) under artificial solar radiation of up to 8 h~~ours~~ with respect to retention time and peak area, indicating that during this irradiation time, neither adsorption nor degradation by photolysis occurred. This marked a difference with the photolysis result in Fig. 6A, where after 8 h~~ours~~ a 50% diminution of the peak area (Gd-DOTA concentration in water) was observed. The result can be interpreted in terms of the capacity of the carbon to absorb the irradiation, and demonstrates once more that the diminution of the Gd-DOTA concentration in the system is due to photodegradation of Gd-DOTA by the TiO_2 immobilized in the composite.

When Gd-DOTA (1 mg L^{-1}) dissolved in synthetic urine was irradiated in presence of the composite (34 g L^{-1}), the peak area did not change after 8 h~~ours~~ of irradiation, but a broadening of the peak front occurred and the peak shifted slightly to shorter retention times. This finding might be attributed to a slight modification of the Gd-DOTA chelate or to chromatographic interferences by components of the synthetic urine. Neither substantial photodegradation of Gd-DOTA by irradiation nor adsorption of Gd-DOTA on the composite could be observed using synthetic urine as matrix. Our previous report on the adsorption of Gd-DOTA also demonstrated poor adsorption of Gd-DOTA on activated carbon in a synthetic urine matrix (Elizalde-González et al., 2017).

3.4 Adsorption-desorption of ionic gadolinium species

Fig. 8 shows chromatograms depicting the behavior of the irradiated Gd-DOTA solution in the photocatalytic experiment with the composite under artificial solar irradiation. Under these conditions, the HPLC-ICP-MS chromatograms of the aqueous solution of Gd-DOTA showed peaks corresponding to Gd-containing photodegradation products formed after 8 h~~ours~~ of irradiation (Fig. 8B). One of the possible results of the phototransformation of Gd-DOTA is the partial rupture of the Gd-DOTA complex, releasing free gadolinium. As a result, the products contained in the solution may include gadolinium or fragments of the ligand DOTA.

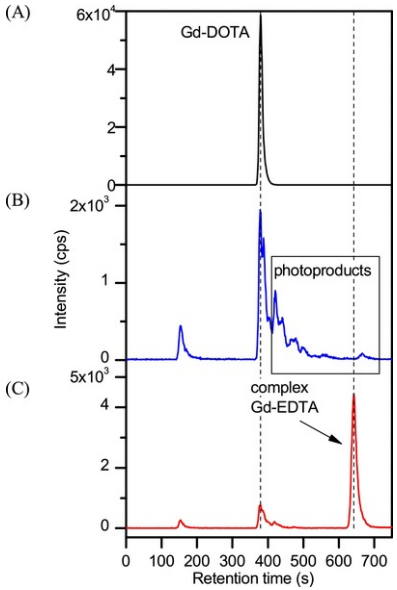

Fig. 8 HPLC-ICP-MS chromatograms of an initial aqueous solution of Gd-DOTA (1 mg L^{-1}) (A), after 8 h exposure to artificial solar light in presence of the TiO_2/Carbon composite (B) and resultant solution after desorption of adsorbed Gd transformation products (C). Desorbed free Gd^{3+} was complexed by addition of EDTA.

alt-text: Fig. 8

To explain the time-dependent decrease of Gd-DOTA concentrations presented in Fig. 6 measured by IEC-ICP-MS on *m/z* 157 (Gd), it can be surmised that other Gd-containing compounds, transformation products and free gadolinium could be trapped by the composite. Thus, to prove this hypothesis, the possibly adsorbed gadolinium species were forced to desorb as described in the experimental section. To detect free Gd^{3+} by anion exchange chromatography, it has to be converted into a negatively charged new complex by the addition of EDTA to the desorption solution.

The identification of the Gd-DOTA and the Gd-EDTA complex by molecular mass was carried out by parallel detection with ESI/QToF-MS. Fig. 8C shows the Gd-EDTA peak at retention time 642 s, well-separated from that of Gd-DOTA at retention time 379 s. The respective mass spectrum of Gd-EDTA exhibited signals at *m/z* 508.02 $[M + CH_3COOH+H]^+$ and 447.99 $[M+H]^+$, corresponding to $C_{12}H_{18}GdN_2O_{10}^+$ (Gd-EDTA + CH_3COOH) and $C_{10}H_{14}GdN_2O_8^+$ (Gd-EDTA). This result indicates that Gd-DOTA can be partially degraded to strong anionic Gd-containing complexes (Fig. 8B) as well as to weak Gd- complexes or free gadolinium cation (Gd^{3+}) (Please check the size on the left and right side of this parenthesis.) adsorbed-desorbed by the composite. The latter Gd-species can be transcomplexed or complexed in the presence of EDTA and separated by anion exchange chromatography.

As demonstrated by Qadeer et al.(1992); Chen et al. (2014); and Li et al.(2015) the adsorption of Gd^{3+} is feasible on carbonaceous adsorbents. They all reported that adsorption of Gd^{3+} on activated charcoal, graphene oxide and chitosan/carbon, respectively, is higher in slight acidic solution than in strong acidic solution. Thus, our result confirms the removal of free gadolinium by the TiO_2/Carbon composite, but it is not possible to conclude whether the sorption localizes on the surface of carbonaceous zones or on TiO_2 particles, or both. Evidence of the interaction between rare earth elements like Gd^{3+} and TiO_2 is provided in several works (Dai et al., 2009). Nanometer–size TiO_2 has been used successfully in the pre-concentration of rare earth elements via adsorption (Liang et al., 2001; Xu et al., 2009; Paul et al., 2015), and Gd^{3+} adsorbs in a wide pH-range on titanium dioxide rutile phase via hydrolyzed surface species (Piasecki and Sverjensky, 2008). A TiO_2-graphene oxide composite has also been used to adsorb some target rare earth elements (Zhang et al., 2015).

3.5 Identification of photochemically induced transformation products of Gd-DOTA

The photocatalytic degradation of Gd-DOTA was analyzed by anion exchange chromatography coupled simultaneously with ICP-MS and ESI-QToFMS as detectors. Besides the initial Gd-DOTA complex, numerous Gd - containing chromatographic peaks could be detected in the ICP-MS chromatograms (as an example, see Fig. 8B, *m/z* $^{157}Gd^+$). Their exact molar mass (mass to charge ratio *m/z*) could be determined in parallel by means of the typical isotopic pattern of gadolinium in the ESI-MS spectra observed in the extracted ion chromatograms (EIC) in Fig. 9A.

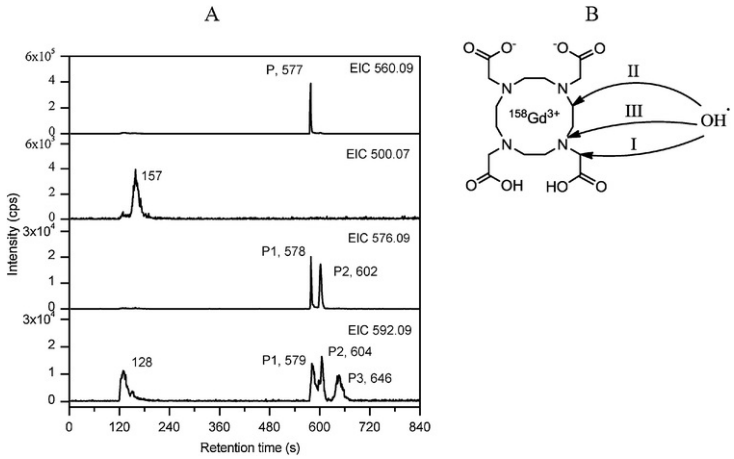

Fig. 9 Selected ion extracted chromatograms (ESI-QToFMS) (A) of Gd-DOTA and its main Gd-containing transformation products (all *m/z* as $(M+H)^+$ with $^{158}Gd^{3+}$ and possible points of attack to the ligand in Gd-DOTA complex by photocatalytically induced OH-radicals (B).

alt-text: Fig. 9

In Table 3 the identified peaks with their formula, ion formula, accurate *m/z* (observed and calculated), the error (Δppm) and the neutral loss are summarized. The *m/z* of the Gd-containing transformation products are related to the ^{158}Gd isotope. The observed photocatalytic transformation led to two types of Gd - containing products with a remaining intact cyclic tetraazacyclododecane ligand just as in the Gd-DOTA. In the retention time range near the void volume (157 s) a Gd-complex could be identified in which an acetate group of the ligand 1,4,7,10-tetraazacyclododecane-1,4,7,10 tetraacetic acid was cut photocatalytically. Further reaction products were detected at slightly longer retention times than the initial Gd-complex ($[M+H]^+$ *m/z* 560.0986) with two main peaks (P1 and P2) with *m/z* 576.0935 and 3 main peaks (P1-P3) with *m/z* 592.0884. The mass increase of 16 and 32, respectively, in relation to the mass of Gd-DOTA (*m/z* 560.0986), suggested that an oxidation of the ligand occurred by attachment of hydroxyl radicals as seen in Fig. 9B.

Table 3 Identification of the original Gd-complex, selected photolysis products and their typical MS/MS fragments.

alt-text: Table 3

Gd-Complex	Molecular composition		Complex identification			Fragment identification[c]				
Ligand	[M]	$[M+H]^+$	Calc. *m/z*	Obs. *m/z*	Error[a] Δppm	Calc. *m/z*	Obs. *m/z*	Error[a] Δppm	Neutral loss	Peak[b]
DOTA	$C_{16}H_{25}GdN_4O_8$	$C_{16}H_{26}GdN_4O_8^+$	560.0986	560.1004	3.2	516.1088	516.1118	5.8	-44 (CO_2)	^{560}P
DOTA + O	$C_{16}H_{25}GdN_4O_9$	$C_{16}H_{26}GdN_4O_9^+$	576.0935	576.0954	3.3	502.0931	502.0923	1.6	-74 ($C_2H_2O_3$)	^{576}P1 A[c]
			576.0935	576.0952	3.0	532.1037	532.1016	3.9	-44 (CO_2)	^{576}P1B[c]
						558.0830	558.0808	3.9	-18 (H_2O)	^{576}P2
DOTA+2O	$C_{16}H_{25}GdN_4O_{10}$	$C_{16}H_{26}GdN_4O_{10}^+$	592.0884	592.0910	3.7	548.0986	548.0984	0.4	-44 (CO_2)	^{592}P1
						460.1190	460.1163	5.9	-132 (3xCO_2)	^{592}P1
			592.0884	592.0877	1.2	518.0881	518.0827	9.2	-74 ($C_2H_2O_3$)	^{592}P1, P2
						516.0724	516.0733	1.7	-76 ($C_2H_4O_3$)	^{592}P2
			592.0884	592.0899	2.5	556.0673	556.0700	4.8	-36 (2xH_2O)	^{592}P3
DOTA-Hac	$C_{14}H_{21}GdN_4O_6$	$C_{14}H_{22}GdN_4O_6^+$	500.0775	500.0790	3.0	412.0978	412.1016	9.2	-88 (2xCO_2)	^{500}P

[a] Error Δppm (MS) <5 ppm, Error Δppm (MSMS) <10 ppm.

[b] iIn ~~Fig. 8~~Fig. 9 where the EIC chromatogram of photolysis products with their exact masses (*m/z*, $[M+H]^+$) and retention times (s) are shown.

[c] A and B indicate different fragmentation paths found for $^{576}P1$.

To identify the probable structures of these compounds, MS/MS fragmentation studies using Q-ToFMS were performed. For the product of photolysis with the positive ion $[M+O+H]^+$ the oxidative attachment of OH-radicals can take place on three different sides of the ligand: (I) on the acetate side chain to form a glycolate side chain from it; (II) on the CH_2-group of the ring to form an alcoholic group (1,4,7,10-tetraazacyclododecan-2-ol-1,4,7,10 tetraacetic acid) or (III) on the tertiary amine to form an amine oxide group (1,4,7,10-tetraazadodecane 1-oxide as illustrated in Fig. 9B. The first mechanism (oxidation of the acetate side chain) was identified by the elimination of glyoxalic acid ($C_2H_2O_3$, *m/z* 74) followed by a triple neutral loss of *m/z* 44 (CO_2). This fragmentation scheme is representative for peak P1, where the oxidation product seems to be 1,4,7,10-tetraazacyclododecane-1,4,7 triacetic acid-10 glycolic acid as chelator for Gd^{3+}. Additionally, a further typical fragment could be found for the above mentioned ligand of 1,4,7,10-tetraazacyclododecane-1,4,7 triacetic acid-10 ethanol by elimination of CO_2 of the glycolic acid side chain. Further fragments containing this ethanolamine structure unit could be identified in the MS/MS spectra of peak P1. A third fragmentation type started with the loss of an acetic acid group to form 1,4,7,10-tetraazacyclododecane-1,4 diacetic acid-10 glycolic acid.

The MS/MS peak spectrum of the second peak (P2) of ~~m/z~~ *m/z* 576 is different from the first peak of the same ~~m/z~~ *m/z* so that an isomeric structure can be suspected. In this case the fragmentation starts with a neutral loss of water to form a fragment with *m/z* 558.083 resulting in a DOTA ligand containing a double bond in the tetraazacyclododecane unit (1,4,7,10-tetraazacyclodocec-5-ene).

The further fragmentation is according to the scheme of neutral loss of CO_2 on the acetate side chains. In a smaller degree, an additional third fragmentation way can be observed beginning with a loss of water from an acetate group of the fragment *m/z* 558.083 where a 2-amino-ethen-1-on side chain is formed. While maintaining this structural unit, the molecule is further dismantled by the neutral loss of three CO_2. Proposed structures selected of the MS/MS fragmentation are summarized in Table 4.

Table 4 Structural proposal for typical MSMS fragments of Gd-DOTA and photocatalytic generated Gd-containing products.

alt-text: Table 4

Precursor Ion (*m/z*)	(*m/z*) of the product ions and structure		
560.0986	516.1088 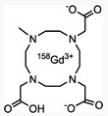		
576.0935	502.0931 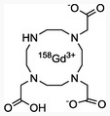	532.1037 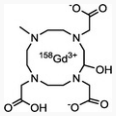	558.0830 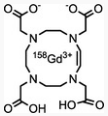
592.0884	548.0986 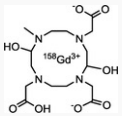	460.119 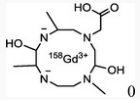	518.0881 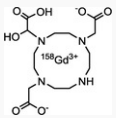
	516.0724 (Please resize this structure (if possible). The cycle appears larger than the other structures.) 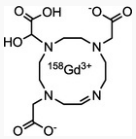	556.0673 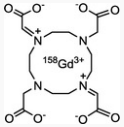	556.0673 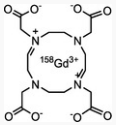
500.0775	412.0978 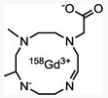		

In the case of the transformation products with ~~m/z~~ m/z 592.0884 ($[M+2O+H]^+$) it can be assumed that the addition of oxygen took place on the same three sides in the molecule but twice. However, this results in further isomeric structures which cannot be completely resolved under these ion chromatographic conditions. The three main peaks (P1-P3) with ~~m/z~~ m/z 592.09 are also partly overlapped. The fragmentation behavior under different dissociation conditions of free DOTA as well Gd-DOTA has been described in detail recently by Beck et al. (2017).

4 Conclusion

The prepared TiO2/Carbon composite exhibited photodegradation efficiency toward one emerging contaminant, Gd-DOTA contrast agent used in magnetic resonance imaging, regardless of the moderate content of the TiO2 semiconductor immobilized on and in the porous guava carbon. The experiments show that Gd-DOTA can be decomposed to 95% in the presence of the proposed composite using artificial solar irradiation. With respect to reaction kinetics, the photocatalytic transformation is still slower than with the nanoparticular TiO_2 suspension. From the technical perspective of abscission and reuse, the TiO2/Carbon composite has the advantage that elaborated centrifugation or filtration procedures can then be omitted. However, further optimization of the preparation of a more efficient composite material has to be given even more attention e.g. by reaching a denser TiO_2 coating/distribution on the composite surface. Using liquid chromatography with ICP-MS and ESI-QTof/MS detection, we demonstrated that photodegradation occurred efficiently by irradiation with artificial solar light and stirring with air bubbles. Diverse photoproducts including free gadolinium tagged by EDTA could be revealed, and some others have yet to be reported. Adsorbed gadolinium species could also be desorbed from the composite. This approach using combined photocatalysis-adsorption-desorption was possible with the proposed TiO_2/Carbon composite, and serves in the development of novel devices useful for the effective elimination of contrast agents.

Acknowledgments

We thank Ursula Bentrup (Leibniz Institute for Catalysis, University of Rostock, Germany) and Patricia Ruíz (CQ-ICUAP, Puebla, Mexico) for performing the Raman and FTIR/DRS analysis, respectively. Eric Reyes Cervantes (CUVyTT, BUAP, Puebla, Mexico) and Javier Martínez Juárez (CDS, ICUAP, Puebla, Mexico) for access to the SEM-EDS and the X-ray fluorescence apparatus, respectively. This work was supported by the following research projects: PROALMEX — CONACyT 165431-2012, Cátedra CONACyT 1001 (2014) and CONACyT INFR-2015-01 252847. MAGM is grateful for the fellowship (304680) received from ~~CONACyT~~CONACyT. The sponsors had no involvement in the study design; collection, analysis and interpretation of data; in the writing of the report; and in the decision to submit the article for publication.

References

Aga D.S., Fate of ~~pharmaceuticals in the environment and in water treatment s~~Pharmaceuticals in the Environment and in Water Treatment Systems, 2008, CRC Press; Boca Raton.

Alipour M., Friedmann D., Scott J. and Amal R., TiO_2/porous adsorbents: ~~R~~recent advances and novel applications, ~~.~~*J. Hazard. Mater.* **341**, 2018, 404–423.

Asahi R., Morikawa T., Ohwaki T., Aoki K. and Taga Y., Visible-light photocatalysis in nitrogen-doped titanium oxides, *Science* **293**, 2001, 269–271.

Bau M., Knappe A. and Dulski P., Anthropogenic gadolinium as a micropollutant in river waters in Pennsylvania, and in Lake Erie, northeastern United States, *Chem. Erde Geochem.* **66**, 2006, 143–152.

Beck S., Trog S., Knizia S. and Linscheid W.M., Fragmentation behavior of DOTA complexes under different activation conditions, *J. Mass Spectrom.* **52**, 2017, 442–451.

Birka M., Wehe C.A., Hachmüller O., Sperling M. and Karst U., Tracing gadolinium-based contrasts agents from surface water to drinking water by means of speciation analysis, *J. Chromatogr. A* **1440**, 2016a, 105–111.

Birka M., Roscher J., Holtkamp M., Sperling M. and Karst U., Investigating the stability of gadolinium based contrast agents towards UV radiation, *Water Res.* **91**, 2016b, 244–250.

Boehm H.P., Surface oxides on carbon and their analysis: a critical ~~A~~assessment, *Carbon* **40**, 2002, 145–149.

Chen W., Wang L., Zhuo M., Liu Y., Wang Y. and Li Y., Facile and highly efficient removal of trace Gd(III) by adsorption of colloidal graphene oxide suspensions sealed in dialysis bag, *J. Hazard. Mater.* **279**, 2014, 546–553.

Cyris M., Behavior of Gadolinium-~~based diagnostics in water t~~Based Diagnostics in Water Treatment, 2013, Diss. Universität Duisburg-Essen; Germany, 2013.

Dai K., Peng T., Chen H., Liu J. and Zan L., Photocatalytic degradation of commercial phoxim over La-doped TiO_2 nanoparticles in aqueous suspension, *Environ. Sci. Technol.* **43**, 2009, 1540–1545.

Ding Z., Hu X., Yue P.L., Lu G.K. and Greenfield P.F., Synthesis of anatase TiO_2 supported on porous solids by chemical vapor deposition, ~~;~~*Catal. Today* **68**, 2001, 173–182.

DRUGBANK 2017 (updated 11.06.2017) https://www.drugbank.ca/drugs/DB09132 (online 20.06.2017).

Elizalde-González M.P. and Hernández-Montoya V., Guava seed as an adsorbent and as a precursor of carbon for the adsorption of acid dyes, *Biores. Technol.* **100**, 2009, 2111–2117.

Elizalde-González M.P., García-Díaz E., González-Perea M. and Mattusch J., Removal of ~~Gadolinium-Based Contrast Agents: A~~gadolinium based contrast agents: adsorption on activated carbon, *Environ. Sci. Pollut. Res.* **24**, 2017, 8164–8175.

EMA/457616/2017 http://www.ema.europa.eu/ema/index.jsp?curl=pages/news_and_events/news/2017/07/news_detail_002780.jsp&mid=WC0b01ac058004d5c. (~~e~~Consulted on 01.08.2018).

Ermolenko N.F. and Yatsevskaya M.M., Investigation of the structure and sorption properties of titan-carbons, *Zhur. Fiz. Khim.* **44**, 1970, 189–193, [in Russian].

~~).~~**Fiol and Villaescusa, 2009** N. Fiol and I. Villaescusa, Determination of sorbent point zero charge: ~~U~~usefulness in sorption studies, *Environ. Chem. Lett.* **7**, 2009, 79–84.

Foratirad H., Baharvandi H.R. and Maragheha M.G., Chemo-rheological behavior of aqueous titanium carbide suspension and evaluation of the gelcasted green body properties, *Mat. Res.* **20**, 2017, 175–182.

Frank O., Zukalova M., Laskova B., Kürti J., Koltai J. and Kavan L., Raman spectra of titanium dioxide (anatase, rutile) with identified oxygen isotopes (16, 17, 18), *Phys. Chem. Chem. Phys.* **14**, 2012, 14567–14572.

Gao Q., Xie J.F., Shao Y.T., Chen C., Han B., Xia K.S. and Zhou C.G., Ultrafast and high-capacity adsorption of Gd(III) onto inorganic phosphorous acid modified mesoporous SBA-15, *Chem. Eng. J.* **313**, 2017, 197–206.

Giles C.H., MacEwan T.H., Nakhawa S.N. and Smith D., Studies in adsorption. Part XI. A system of classification of solution adsorption isotherms, and its use in diagnosis of adsorption mechanisms and in measurement of specific surface areas of solids, *J. Chem. Soc.* **3**, 1960, 3973.

González-Guerrero A.B., Mendoza E., Pellicer E., Alsina F., Fernández-Sánchez C. and Lechuga L.M., Discriminating the carboxylic groups from the total acidic sites in oxidized multi-wall carbon nanotubes by means of acid–base titration, *Chem. Phys. Lett.* **462**, 2008, 256–259.

Jaeger D. and Patscheider J., A complete and self-consistent evaluation of XPS spectra of TiN, *J. Electron. Spectrosc. Relat. Phenom.* **185**, 2012, 523–534.

Khaki M.R.D., Shafeeyan M.S., Raman A.A.A. and Daud W.M.A.W., Application of doped photocatalysts for organic pollutant degradation - ~~A~~a review, *J. Environ. Manag~~e~~.* **198**, 2017, 78–94.

Khalid N.R., Majid A., Bilal Tahir M., Niaz N.A. and Khalid S., Carbonaceous-TiO_2 nanomaterials for photocatalytic degradation of pollutants: ~~A~~a review, *Ceramics Int.* **43**, 2017, 14552–14571.

Kovalova L., Siegrist H., Von Gunten U., Eugster J., Hagenbuch M., Wittmer A., Moser R. and McArdell C.S., Elimination of micropollutants during post-treatment of hospital wastewater with powdered activated carbon, ozone and UV, *Environ. Sci. Technol.* **47**, 2013, 7899–7908.

Kuroda K., Itten R., Kovalova L., Ort C., Weissbrodt D.G. and McArdell C.S., ~~High-technology metals as emerging contaminants: S~~s~~trong increase of anthropogenic gadolinium levels in tap water of Berlin, Germany, from 2009 to 2012~~ (The correct title of this publication is: Hospital-use pharmaceuticals in Swiss waters modeled at high spatial resolution), *Environ. Sci. Technol.* **50**, 2016, 4742–4751.

Lawrence M.G., Ort C. and Keller J., Detection of anthropogenic gadolinium in treated wastewater in South East Queensland~~Australia.~~, Australia, *Water Res.* **43**, 2009, 3534–3540.

Li K., Gao Q., Yadavalli G., Shen X., Lei H., Han B., Xia K. and Zhou C., Selective ~~A~~adsorption of Gd^{3+} on a magnetically retrievable ~~I~~imprinted chitosan/carbon nanotube composite with high capacity, *ACS Appl. Mater. Interf.* **7**, 2015, 21047–21055.

Liang P., Hu B., Jiang Z., Qin Y. and Peng T., Nanometer-sized titanium dioxide micro-column on-line preconcentration of La, Y, Yb, Eu, Dy and their determination by inductively coupled plasma atomic emission spectrometry, *J. Anal. At. Spectrom.* **16**, 2001, 863–866.

Luttrell T., Halpegamage S., Tao J., Kramer A., Sutter E. and Batzill M., Why is anatase a better photocatalyst than rutile? - Model studies on epitaxial TiO_2 films, *Sci. Rep.* **4**, 2014, 4043.

Matos J., Laine J. and Herrmann J.M., Synergy effect in the photocatalytic degradation of phenol on a suspended mixture of titania and activated carbon, *Appl. Catal. B: Environ.* **18**, 1998, 281–291.

Matos J., Garcia-Lopez E., Palmisano L., Garcia A. and Marci G., Influence of activated carbon in TiO_2 and ZnO mediated photo-assisted degradation of 2-propanol in gas–solid regime, *Appl. Catal. B: Environ.* **99**, 2010, 170–180.

Matos J., Miralles-Cuevas S., Ruíz-Delgado A., Oller I. and Malato S., Development of TiO_2-C photocatalysts for solar treatment of polluted water, *Carbon* **122**, 2017, 361–373.

Parfitt G.D. and Rochester C.H., Adsorption from ~~solution at the solid/liquid i~~Solution at the Solid/Liquid Interface, 1983, Academic Press; London, p. 11.

Paul S., Chetri P., Choudhury B., Ahmed G.A. and Choudhury A., Enhanced visible light photocatalytic activity of ~~Gadolinium doped nanocrystalline titania: A~~gadolinium doped nanocrystalline titania: an experimental and theoretical study, *J. Colloid Interf. Sci.* **439**, 2015, 54–61.

Piasecki W. and Sverjensky D.A., Speciation of adsorbed yttrium and rare earth elements on oxide surfaces, *Geochim. Cosmochim. Acta* **72**, 2008, 3964–3979.

Qadeer R., Hanif F., Saleem M. and Afzal M., Adsorption of gadolinium on activated charcoal from electrolytic aqueous solution, *J. Radioanal. Nucl. Chem.* **159**, 1992, 155–165.

Rabiet M., Brissaud F., Seidel J.L., Pistre S. and Elbaz-Poulichet F., Positive gadolinium anomalies in wastewater treatment plant effluents and aquatic environment in the Hérault watershed (South France), *Chemosphere* **75**, 2009, 1057–1064.

Sekiya T., Ohta S., Kamei S., Hanakawa M. and Kurita S., Raman spectroscopy and phase transition of anatase TiO_2 under high pressure, *J. Phys. Chem. Solids* **62**, 2001, 717–721.

Shah M.S.A.S., Park A.R., Zhang K., Park J.H. and Yoo P.J., Green synthesis of biphasic TiO_2–reduced graphene oxide nanocomposites with highly enhanced photocatalytic activity, *Appl. Mater. Interf.* **4**, 2012, 3893–3901.

Soyer P., Dohan A., Patkar D. and Gottschalk A., Observational study on the safety profile of gadoterate meglumine in 35,499 patients: ~~T~~the secure study, *J. Magn. Reson. Imaging* **45**, 2017, 988–997.

Telgman L., Wehe C.A., Birka M., Künnemeyer J., Nowak S., Sperling M. and Karst U., Speciation and isotope dilution analysis of gadolinium-based contrast agents in wastewater, *Environ. Sci. Technol.* **46**, 2012, 11929–11936.

Tepe N., Romero M. and Bau M., High-technology metals as emerging contaminants: ~~S~~strong increase of anthropogenic gadolinium levels in tap water of Berlin, Germany, from 2009 to 2012, *Appl. Geochem.* **45**, 2014, 191–197.

Thommes M., Kaneko K., Neimark A.V., Olivier J.P., Rodriguez-Reinoso F., Rouquerol J. and Sing K.S.W., Physisorption of gases, with special reference to the evaluation of surface area and pore size distribution (IUPAC ~~Technical R~~technical report), *Pure Appl. Chem.* **87**, 2015, 1051–1069.

Uchida H., Itoh S. and Yoneyama H., Photocatalytic decomposition of propyzamide using TiO_2 supported on activated carbon, *Chem. Lett.* **22**, 1993, 1995–1998.

Uchôa-thomaz A.M.A., Sousa E.C., Carioca J.O.B., De Morais S.M., De Lima A., Martins C.G., Alexandrino C.D., Ferreira P.A.T., Rodrigues A.L.M., Rodrigues S.P., De Albuquerque Thomaz J.C., Do Nascimento Silva J. and Rodrigues L.L., Chemical composition, fatty acid profile and bioactive compounds of guava seeds (Psidium guajava L.), *Food Sci. Technol. (Campinas)* **34** (3), 2014, https://doi.org/10.1590/1678-457x.6339.

Vijayalakshmi K. and Sivaraj D., Synergistic antibacterial activity of barium doped TiO_2 nanoclusters synthesized by microwave processing, *RSC Adv.* **6**, 2016, 9663–9671.

Wagner B., Drel V. and Gorin Y., Pathophysiology of gadolinium-associated systemic fibrosis, *Am ~~J Physiol Renal Physio~~. J. Physiol. Renal Physiol.* **311**, 2016, F1–F11.

Xie Z., Guan W., Ji F., Song Z. and Zhao Y., Production of biologically activated carbon from orange peel and landfill leachate subsequent treatment technology, *J. Chem.* 2014, 1–9, https://doi.org/10.1155/2014/491912, ID 491912.

Xu J., Ao Y., Fu D. and Yuan C., Synthesis of Gd-doped TiO_2 nanoparticles under mild condition and their photocatalytic activity, *Colloid Surf. A* **334**, 2009, 107–111.

Yantasee W., Fryxell G.E., Porter G.A., Pattamakomsan K., Sukwarotwat V., Chouyyok W., Koonsiripaiboon V., Xu J. and Raymond K.N., Novel sorbents for removal of gadolinium-based contrast agents in sorbent dialysis and hemoperfusion: ~~P~~preventive approaches to nephrogenic systemic fibrosis, *Nanomed. Nanotechnol.* **6**, 2010, 1–8.

Zeng J., Liu S., Cai J. and Zhang L., TiO_2 ~~I~~immobilized in cellulose matrix for photocatalytic degradation of phenol under weak UV light irradiation, *J. Phys. Chem. C* **114**, 2010, 7806–7811.

Zhang J., Zhou P., Liu J. and Yu J., New understanding of the difference of photocatalytic activity among anatase, rutile and brookite TiO2, *Phys. Chem. Chem. Phys.* **16**, 2014, 20382-20382.

Zhang Y., Zhong C., Zhang Q., Chen B., He M. and Hu B., Graphene oxide-TiO_2 composite as a novel adsorbent for the preconcentration of heavy metals and rare earth elements in environmental samples followed by on-line inductively coupled plasma optical emission spectrometry detection, *RSC Adv.* **5**, 2015, 5996–6005.

Zhu Y., Hoshino M., Yamada H., Itohand A. and Haraguchi H., Gadolinium anomaly in the distributions of the rare earth elements observed for coastal seawater and river waters around Nagoya City, *Bull. Chem. Soc. Jpn.* **77**, 2004, 1835–1842.

Graphical abstract

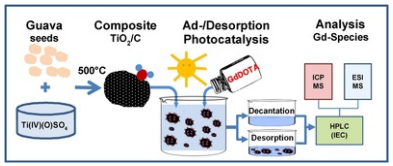

Highlights

- New composite consisting of guava carbon impregnated with TiO_2 is multifunctional.
- Elemental/molecular characterisation of TiO_2/Carbon composite.
- Observing fast and complete photodegradation of Gd-DOTA via intermediates formation.
- Photocatalytical degradation and adsorption of Gd-DOTA allows recuperation of Gd.
- Analysis of Gd-transformation products by IC coupled to ICP-MS and ESI-QToF-MS~~ABSTRACT~~.

Queries and Answers

Query: Fig. 1 will appear in black and white in print and in color on the web. Based on this, the respective figure caption has been updated. Please check, and correct if necessary.
Answer: The update of the figure caption is correct

Query: The author names have been tagged as given names and surnames (surnames are highlighted in teal color). Please confirm if they have been identified correctly.
Answer: Yes

Query: Please check the designated corresponding author, and correct if necessary.
Answer: corresponding author is correct

Query: Please check the email address for corresponding author, and correct if necessary.
Answer: Address is correct

Query: Please confirm that the provided email maria.elizalde.uap.mx@gmail.com is the correct address for official communication, else provide an alternate e-mail address to replace the existing one, because private e-mail addresses should not be used in articles as the address for communication.
Answer: maria.elizalde@correo.buap.mx

Query: Your article is registered as a regular item and is being processed for inclusion in a regular issue of the journal. If this is NOT correct and your article belongs to a Special Issue/Collection please contact d.mahoney@elsevier.com immediately prior to returning your corrections.
Answer: Article is regular

Query: Have we correctly interpreted the following funding source(s) and country names you cited in your article: PROALMEX — CONACyT, Cátedra CONACyT 1001 (2014), CONACyT INFR-2015-01

252847, CONACyT?

Answer: Yes